IPP-Report

MAX-PLANCK-INSTITUT
FÜR PLASMAPHYSIK

Hartmut Zohm

Forced Rotation of Tearing Modes by Time Varying RMP Fields

IPP 2022-06
September 2022

Forced Rotation of Tearing Modes by Time Varying RMP Fields

Hartmut Zohm

DEMO Central Team, EUROfusion PMU, Boltzmannstr. 2, D-85748 Garching
Max-Planck-Institut für Plasmaphysik, Boltzmannstr. 2, D-85748 Garching

1.) Introduction

The occurrence of tearing modes limits the operational space of tokamaks in density and radiative losses (in both cases triggered by the current gradient, 'classical' tearing modes) as well as achievable beta (pressure driven, 'neoclassical' tearing modes), with the islands occurring on resonant surfaces reducing the confinement, often also leading to disruptive termination of the discharge. A possible countermeasure is to drive local currents at the resonant surface by Electron Cyclotron Current Drive (ECCD), preferably in the O-point of the magnetic island. In present day experiments, initially rotating tearing modes are often observed to lock in the laboratory frame, which is explained by a slowing down due to eddy currents induced in the vacuum vessel wall and then a phase locking to the helical component of the unavoidable error field due to imperfect shape and positioning of the coil system or its feeds (see e.g. [1]). Since it is not guaranteed that the locked phase position is compatible with O-point injection through the ECCD launcher, it is proposed for future large tokamaks to use active coil sets producing helical components (Resonant Magnetic Perturbation, RMP) to move the locked mode into the optimum position for stabilization. The principal feasibility of this scheme has been demonstrated experimentally [2] and control has been discussed in [3] and [4]. The aim of this contribution is to identify the time scales for this process and to derive a criterion for the RMP strength depending on the required time scale for the forced rotation. An application on EU-DEMO is discussed.

2.) The model

We describe the mode dynamics by a momentum balance equation taking into account viscous drag, the force due to eddy currents in the resistive wall and the force due to interaction with an external helical field. We chose a simple cylindrical geometry and neglect the toroidal component of the perturbed field. In this model, the mode interacts only with the component of the error field that has the same single helicity, so that the external field mimicks both the error field as well as the (externally controlled) RMP field. The evolution of the island width is modelled by a modified version of the Rutherford equation, taking into account the effect of the RMP on the island width, but neglecting small island effects since we are only interested in the locking of modes of appreciable size. The model is described in the following two sections, and the detailed expressions for the different terms can be found in [1].

2.1) Momentum balance

The momentum balance consists of the following forces that are assumed to lead to a toroidal torque at $R=R_0$, the tokamak major radius:

$$F_{visc} = m_p R_0 \frac{(\omega_0 - \omega)}{\tau_M} \tag{1}$$

is the viscous force that pulls the rotation frequency ω back to the 'natural' rotation frequency ω_0 on the momentum confinement time scale τ_M. Here, m_p is the mass of the plasma involved, and we assume that it is the whole plasma mass, although on time scales much smaller than τ_M, one may argue that initially, it is only the mass in the island. Next, we add the drag due to the resistive wall

$$F_{wall} = -\frac{\pi^2 R_0 m^2 W^4}{64\mu_0 r_s}\left(\frac{r_s}{r_W}\right)^{2m}\left(B_{0\theta}\frac{q'}{q}\right)^2 \frac{\omega\tau_W}{1+(\omega\tau_W)^2} \tag{2}$$

where τ_W is the wall time constant for a mode with poloidal mode number m, $B_{0\theta}$ the equilibrium poloidal field and q' the radial derivative of the safety factor q. All quantities are evaluated at the resonant surface r_s. The island is parametrized by the island width W, which is proportional to the square root of the perturbed field B_r

$$W = 4\sqrt{\frac{r_s q B_r}{m q' B_{0\theta}}} \tag{3}$$

where we have calculated W from the unshielded B_r, i.e. neglected the reduction of island width due to the eddy currents in the wall, equivalent to the assumption $(r_s/r_W)^{2m} << 1$.

The force due to the error field is

$$F_{ef} = -\frac{\pi^2 R_0 m^2 W_{ef}^2 W^2}{32\mu_0 r_s}\left(B_{0\theta}\frac{q'}{q}\right)^2 \sin\left(m\left(\theta-\theta_{ef}\right)\right) \tag{4}$$

where θ is the poloidal angle which is related to the instantaneous angular velocity by $\omega = d\theta/dt$ and θ_{ef} is the phase of the error field in the laboratory frame. Here, the strength of the error field has been parametrized by W_{ef}, which is the width of the island that the error field would open up at the resonant surface. As outlined above, applying an RMP of strength W_{RMP} will lead to a similar force, but now the phase of the RMP field, θ_{RMP}, will vary in time when the mode is moved around:

$$F_{RMP} = -\frac{\pi^2 R_0 m^2 W_{RMP}^2 W^2}{32\mu_0 r_s}\left(B_{0\theta}\frac{q'}{q}\right)^2 \sin\left(m\left(\theta-\theta_{RMP}(t)\right)\right) \tag{5}$$

We now set up the toroidal torque balance, using the fact that the electromagnetic forces are mainly in the poloidal direction and the toroidal torque is 1/q smaller than the poloidal torque

$$m_p R_0^2 \frac{d\omega}{dt} = R_0\left(F_{visc} + \frac{1}{q}\left(F_{wall}+F_{ef}+F_{RMP}\right)\right) \tag{6}$$

We then introduce another characteristic time scale, namely the Alfvén time scale τ_A, that describes the (small) plasma inertia

$$\tau_A = \sqrt{\frac{64 m_p \mu_0}{\pi^2 r_s B_{0\theta}^2}} \tag{7}$$

Where the unusual numerical factor $64/\pi$ has been included for the sake of simplicity in what follows. In the last step, we normalize the angular frequency by the natural frequency, time by the wall time constant, and the island width by the radius of the resonant surface

$$\widetilde{\omega} = \frac{\omega}{\omega_0}; \qquad \tilde{t} = \frac{t}{\tau_W}; \qquad \widetilde{W} = \frac{W}{r_s}; \tag{8}$$

so that the torque balance in dimensionless form reads

$$\frac{d\widetilde{\omega}}{d\tilde{t}} = \frac{\tau_W}{\tau_M}(1-\widetilde{\omega}) - \frac{m^2 s^2 \widetilde{W}^4}{q\omega_0^2\tau_A^2}\left(\frac{r_s}{r_W}\right)^{2m}\frac{\widetilde{\omega}}{(\omega_0\tau_W)^{-2}+\widetilde{\omega}^2} - 2\omega_0\tau_W\frac{m^2 s^2\widetilde{W}^2}{q\omega_0^2\tau_A^2}\left(\widetilde{W}_{ef}^2\sin\left(m\left(\theta-\theta_{ef}\right)\right)+\widetilde{W}_{RMP}^2\sin\left(m\left(\theta-\theta_{RMP}(\tilde{t})\right)\right)\right) \quad (9)$$

with

$$\widetilde{\omega} = \frac{1}{\omega_0\tau_W}\frac{d\theta}{d\tilde{t}} \quad (10)$$

Here, the mode amplitude W can in principle be supplied as an arbitrary function of time, but in section 2.3, we will link it to the Rutherford equation. However, some of the limiting cases can be discussed even for constant W, which we will do now.

2.2) Discussion of limiting cases

First, we consider the wall torque slowing down the mode, but not the error field or the RMP. This case is discussed in detail e.g. in [5], where it is shown that due to the nonlinearity of the wall torque, there is the possibility of two co-existing solutions, one at high frequency $\widetilde{\omega} \gg \tau_W$, close to the natural frequency ω_0 and the other at $\widetilde{\omega} \ll \tau_W$. The latter is often not seen in experiments since at such low frequencies, the mode can already be trapped in the error field (see below). The transition between the two states has a bifurcation character. Here, we only deal with cases where the model locks.

Next, we discuss the trapping of the mode in the error field. Without external torque and viscosity, this is equivalent to a mass point moving in a sinusoidal potential and, depending on the initial inertial force ~ $(\tau_A\omega_0)^2$, the mode either rotates at a modulated frequency or oscillates around the equilibrium point θ=θ_0, if $\widetilde{W}_{ef} > \omega_0\tau_A\sqrt{q}/(2ms\widetilde{W})$.

For our problem, the more relevant case is the balance between drive and error field, since it determines the stationary locking point. In stationary state, (9) reduces to

$$0 = \frac{\tau_W}{\tau_M} - 2\omega_0\tau_W\frac{m^2 s^2\widetilde{W}^2}{q\omega_0^2\tau_A^2}\left(\widetilde{W}_{ef}^2\sin\left(m\left(\theta-\theta_{ef}\right)\right)+\widetilde{W}_{RMP}^2\sin\left(m(\theta-\theta_{RMP})\right)\right) \quad (11)$$

Since the sum of two sine functions of same frequency but arbitrary phase and amplitudes is again a sine function, i.e.

$$\widetilde{W}_{tot}^2\sin\left(m(\theta-\theta_{tot})\right) = \widetilde{W}_{ef}^2\sin\left(m\left(\theta-\theta_{ef}\right)\right)+\widetilde{W}_{RMP}^2\sin\left(m(\theta-\theta_{RMP})\right) \quad (12)$$

where the total island width can be expressed as

$$\widetilde{W}_{tot}^2 = \sqrt{\widetilde{W}_{ef}^4+\widetilde{W}_{RMP}^4+2\widetilde{W}_{ef}^2\widetilde{W}_{RMP}^2\cos\left(m\left(\theta_{ef}-\theta_{RMP}\right)\right)} \quad (13)$$

so that the locking phase can calculated by

$$m(\theta-\theta_{tot}) = \sin^{-1}\left(\frac{q\omega_0^2\tau_A^2}{2\omega_0\tau_M m^2 s^2\widetilde{W}^2\widetilde{W}_{tot}^2}\right) \quad (14)$$

One can see that in the case of a large mode/strong RMP field, the mode will lock close to the minimum of the total external helical field, while the mode will be unlocked by the viscous force ~ $(\tau_A\omega_0)^2$ / $(\omega_0\tau_M)$ for $\widetilde{W}_{tot} < \omega_0\tau_A/(ms\widetilde{W})\sqrt{q/(2\omega_0\tau_M)}$. The precise amplitude and phase of the required RMP field will depend on the initially unknown error field and the position of the ECCD launchers. In our model with only one helicity, we can always completely cancel the error field so that the mode will never

completely lock and the problem becomes 'academic', but in reality, the error field and the RMP field will consist of a different spectrum of helical harmonics so that in general, complete compensation is not possible and remains an optimization problem. We come back to this discussion in Section 3.

For our case of moving the phase of a locked mode, it is not only important to consider the amplitude for mode locking, Eqn. (13), but also the dynamic behavior of the system. For this, we note that the inertial and viscous terms can be neglected against the wall drag, and we can move the mode against the wall force by changing the phase θ_{tot} in time if

$$\frac{m^2 s^2 \widetilde{W}^4}{q\omega_0^2\tau_A^2}\left(\frac{r_s}{r_W}\right)^{2m}(\omega_0\tau_W)^2\widetilde{\omega} < 2\omega_0\tau_W\frac{m^2 s^2 \widetilde{W}^2}{q\omega_0^2\tau_A^2}\widetilde{W}_{tot}^2\sin\big(m(\theta-\theta_{tot}(t))\big) \tag{15}$$

where we have used the low frequency approximation of the wall drag term. Using Eqn. (10), this can be transferred into a simple condition for the time scale at which we can move the mode around:

$$\frac{d\theta}{d\tilde{t}} \le 2\left(\frac{r_W}{r_s}\right)^{2m}\left(\frac{\widetilde{W}_{tot}}{\widetilde{W}}\right)^2 \tag{16}$$

Since time is normalized to the wall time, it means that this is the typical time scale. If one tries to move the mode faster, it cannot follow and will 'ratchet' through the sinusoidal potential trapping it (see also discussion in Section 3).

2.3) Mode evolution (Rutherford) equation

In the previous section, we have solved the equation of motion for a prescribed *W(t)*. More consistently, the mode evolution W(t) is described by the modified Rutherford equation (MRE). Since for our problem, we are not interested in the precise dynamics of the mode, we just adopt a version that leads to nonlinear saturation at $W=W_{sat}$, via a *W*-dependence of the stability parameter, $\Delta'(W)$, as is common for describing current driven tearing modes. More importantly for our problem, the external helical field will have an effect on the island width as well, which we take into account by a separate term in the MRE. This term can be stabilizing or destabilizing, depending on the island's phase w.r.t. the total helical field represented according to Eqn. (12) in the following equation:

$$\frac{\tau_R}{\tau_W}\frac{d\widetilde{W}}{d\tilde{t}} = \Delta_0'\left(1-\frac{\widetilde{W}}{\widetilde{W}_{sat}}\right) + 2m\left(\frac{\widetilde{W}_{tot}}{\widetilde{W}+\widetilde{W}_0}\right)^2\cos\big(m(\theta-\theta_{tot})\big) \tag{17}$$

where we have introduced a small island term W_0 to remove the singularity at small island width. This usually involves the layer physics as described e.g. in [1], but here we are only interested in large island sizes. In this limit, we can get a simple relation for the change of saturated island width in the presence of the error field by setting *d/dt* to zero and linearising the resulting cubic equation:

$$\widetilde{W}_{sat,tot} = \widetilde{W}_{sat}\left(1+\frac{2m}{\Delta'}\left(\frac{\widetilde{W}_{tot}}{\widetilde{W}_{sat}}\right)^2\cos\big(m(\theta-\theta_{tot})\big)\right) \tag{18}$$

If needed, the effects of neoclassical drive and ECCD stabilization can be added through the appropriate terms in the MRE. ECCD stabilization could lead to interesting dynamics with the mode unlocking at small *W*, thereby reducing the stabilization efficiency. This will be added in future work.

2.4) Limitations of the model

The model will be used to estimate the typical amplitudes and timescales for DEMO, so it is not meant to give precise quantitative information. However, it is still useful to discuss the main shortcomings and how they can be addressed:

- The model contains only one helical poloidal harmonic in a cylinder. Mode coupling is therefore not included, i.e. any other spectral component will not lead to a net force. This can partly be amended by allowing for a shaped cross section and the resulting non-uniform stepsize of the poloidal angle in the poloidal plane, i.e. considering the cylinder as a map of a shaped cross-section onto straight field lines. This is discussed in the next section for the specification of the error field and its compensation by RMPs.
- At present, the plasma is modelled as a rigid rotator that slows down on the timescale of the momentum confinement time. In reality, the electromagnetic forces act locally on the resonant surface, which then transmits the momentum on the momentum confinement time scale τ_W to the rest of the plasma. Thus, at time scales shorter than τ_W, only the mass contained in the island has to be considered, which is sometimes found in the literature and leads to a different *W*-dependence of the force terms (one power less than we use). This process is not resolved in our model, i.e. experimentally, the modes will lock faster than described here, but the slowing down of the whole plasma should be described better. In order to improve the description to a local one, a momentum diffusion equation would have to be solved in parallel, as was done in [6].
- The absence of rotation profile effects also leads to a potential overestimate of the restoring force (parametrised by balance of momentum confinement time and the 'natural' rotation frequency), since it assumes that the rotation of the resonant surface is equivalent to the average of the plasma momentum over radius. This can be corrected by assuming a momentum density profile, calculating the ratio between local and average momentum density, and then increasing the momentum confinement time by this ratio (i.e. the restoring force is actually lowered, which makes the mode lock faster).
- The 'natural rotation' ω_0 depends on the different terms that generate mode rotation, of which only NBI torque is well known at present. While this term indeed dominates in present day devices, its extrapolation to future large devices is not straightforward since the contribution from the lesser known terms (intrinsic rotation, NTV torque) may dominate there (in fact, DEMO may work without NBI at all).

These points will be taken into account in the next section when we insert numerical values into the equations outlined.

3.) Application to DEMO

For the application to DEMO, the input data for the error field are

- an estimate of the error field on the q=2 surface due to imperfections in the TF and PF coils
- the optimized RMP field for compensation evaluated by TMEI or plasma response criteria

These are provided by F. Villone in a poloidal plane on the q=2 surface for each *n* separately, i.e. contain the effects of toroidicity and shaping. Also provided is the geometry of the q=2 surface. In order to translate these into the cylindrical model, a straight field line approach is provided using an analytical fit to the q=2 surface according to [1]:

$$R(r,\theta) = R_0 + r\cos\theta + \Delta(r) - S_2(r)\cos\theta + S_3\cos 2\theta \tag{19}$$

$$z(r,\theta) = r\sin\theta + S_2(r)\sin\theta - S_3\sin 2\theta \tag{20}$$

where r, θ is a cylindrical co-ordinate system around R_0, Δ is the Shafranov shift, S_2 is related to the elongation κ by $k=(1+S_2/r)/(1-S_2/r)$, S_3 is related to the triangularity δ by $\delta=S_3/(4r)$, and the prime denotes the radial derivative. For this parametrisation the straight field line angle can be given analytically:

$$\theta^* = \theta - \left(\frac{r}{R_0} - \Delta'\right)\sin\theta - \frac{r\kappa'}{(\kappa+1)^2}\sin 2\theta + \frac{1}{12}(r\delta' - \delta)\sin 3\theta \qquad (21)$$

Fig. 1 show the flux surface geometry as well as the shape parameters and the straight field line derived from it at the q=2 surface.

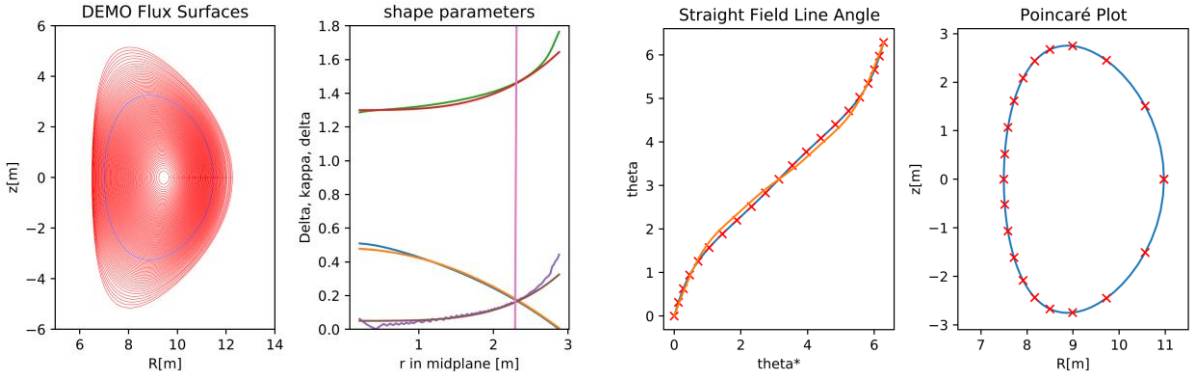

Fig. 1: From left to right: flux surface geometry for EU DEMO (the q=2 surface is marked in blue), shape parameters as function of the radius, and straight field line angle as a function of the geometric poloidal angle w.r.t. the centre of the q=2 surface as well as in a Poincaré plot.

Since both error field and RMP field are given in full toroidal geometry, it is necessary to extract the (2,1) component as our simple cylindrical model only deals with one helical component. Noting that the toroidal mode number n is a good quantum number, the field is provided by F. Villone as a normal component of the n=1 component on the q=2 surface in a poloidal plane as function of the geometric angle. Both fields are then mapped onto the straight field line angle using the transformation given by eqn. (21). Since the RMP field is created by a single toroidal row of coils, see left part of Fig. 2, it can be described by a single real function $B_{RMP}(\theta)$ in the poloidal plane with the whole *n=1* component of the field given by

$$B_{RMP}(\theta,\phi)=B_{RMP}(\theta)\,\sin(\phi-\phi_0) \qquad (22).$$

The function $B_{RMP}(\theta)$ is also shown in Fig. 2 in both the geometrical and the helical angle.

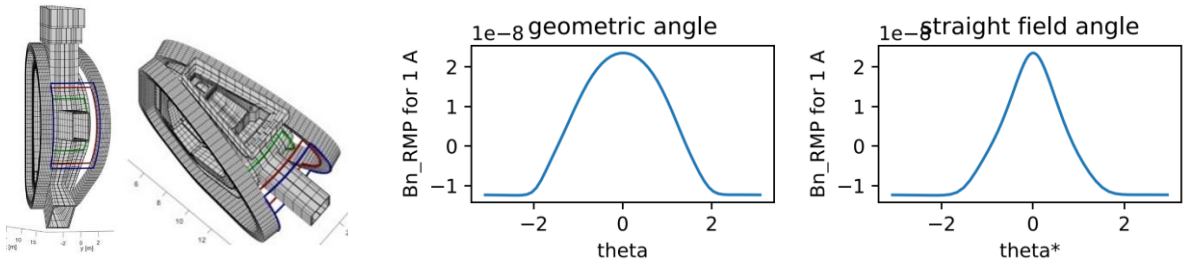

Fig. 2: different conceptual midplane RMP coils for DEMO (left) and the n=1 component produced by the blue variant on the q=2 surface, normalised to the value created by a current of 1 A in the coils. The field is shown in a poloidal plane as a function of both geometric and straight field line angle.

The functional form (22) demonstrates that the RMP field does not have a net helical component, but it can be decomposed into pairs of helical components of opposite helicity and equal magnitude through

$$f(\theta,\varphi) = \frac{a_{00}}{2} + \sum_{m=0}^{\infty}\sum_{n=0}^{\infty}(a_{mn}^{+}\cos(m\theta + n\varphi) + b_{mn}^{+}\sin(m\theta + n\varphi)) + \sum_{m=0}^{\infty}\sum_{n=0}^{\infty}(a_{mn}^{-}\cos(m\theta - n\varphi) + b_{mn}^{-}\sin(m\theta - n\varphi))$$

with

$$a_{mn}^{+} = \frac{2}{(2\pi)^2}\int_{\theta=0}^{2\pi}\int_{\varphi=0}^{2\pi} d\theta d\varphi f(\theta,\varphi)\cos(m\theta + n\varphi)$$

$$b_{mn}^{+} = \frac{2}{(2\pi)^2}\int_{\theta=0}^{2\pi}\int_{\varphi=0}^{2\pi} d\theta d\varphi f(\theta,\varphi)\sin(m\theta + n\varphi)$$

$$a_{mn}^{-} = \frac{2}{(2\pi)^2}\int_{\theta=0}^{2\pi}\int_{\varphi=0}^{2\pi} d\theta d\varphi f(\theta,\varphi)\cos(m\theta - n\varphi)$$

$$b_{mn}^{-} = \frac{2}{(2\pi)^2}\int_{\theta=0}^{2\pi}\int_{\varphi=0}^{2\pi} d\theta d\varphi f(\theta,\varphi)\sin(m\theta - n\varphi)$$

Where θ stands for either the geometric or the straight field line angle. For our case, we only have one toroidal component (n=1), and hence the mode spectrum is fully described by the poloidal mode number m. The first 5 Fourier components of the RMP field are shown in Fig. 3 in both poloidal angles. One can see that in the straight field line angle, significant spectral power is shifted from m=1 to m=2, which shows that it is important to consider the real geometry.

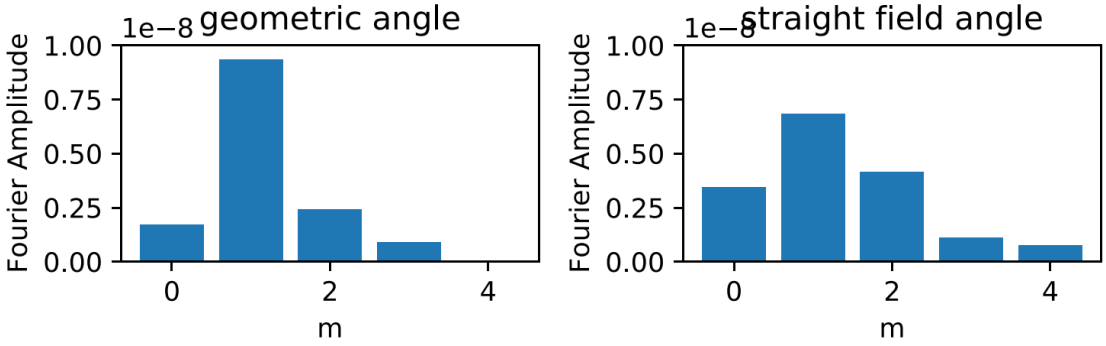

Fig. 3: Poloidal mode spectrum of the n=1 component of the RMP field for the first five harmonics.

The error field is determined by a Monte Carlo simulation of individual errors of the TF and PF coil positions and shapes. Fig. 4 shows a typical result of such a simulation and also the corresponding n=1 component, which is a poor approximation since the error field is due to random perturbation of 16 TF coils, but still represents the most critical component resonant with the plasma.

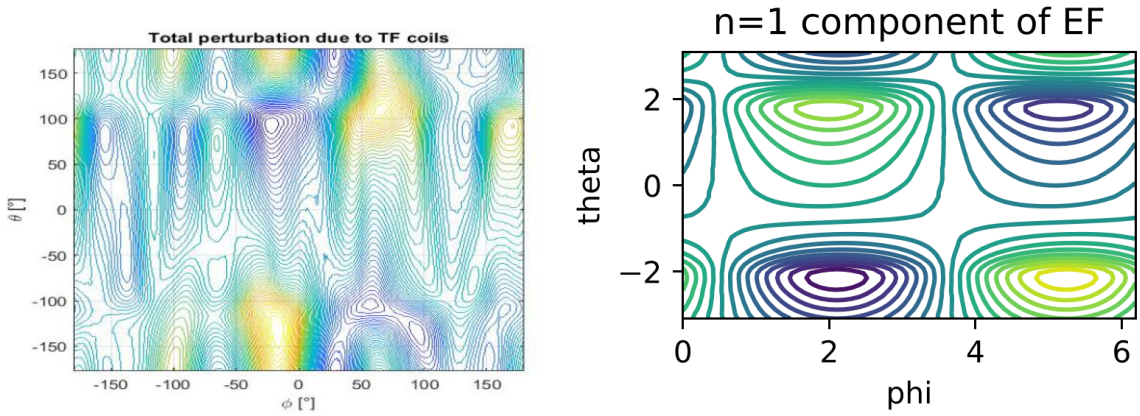

Fig. 4: map of typical error field due to errors in the TF coils (left) and n=1 component thereof (right).

For the error field, a helical component cannot be excluded a priori, and in fact the input given by F. Villone consisted of an n=1 component which is given as $B_{ef}(\theta)$, but has a real and an imaginary part, which, in real space can be visualized as

$$B_{ef,tot} = A(\theta)\cos(\phi - \phi_0(\theta)) \qquad (23)$$

with amplitude $A(\theta) = ((Re(B_{ef}[\theta])]^2+(Im[B_{ef}(\theta)])^2)^{1/2}$ and phase $\phi_0(\theta) = arctan(Im[B_{ef}(\theta)]/Re[B_{ef}(\theta)])$. These functions are shown in Fig. 5.

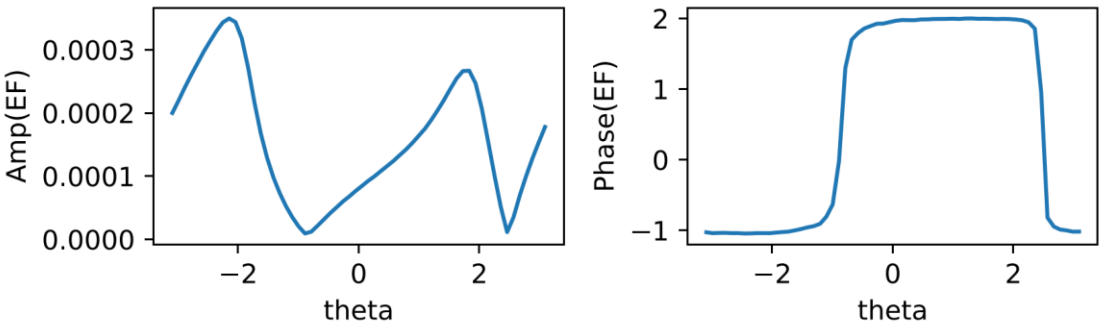

Fig. 5: Amplitude and phase of the n=1 component of the error field in a poloidal plane.

The phase variation shows a more or less constant phase over two sections of the poloidal circumference with a flip by almost π in between. This indicates that in fact the net helical component is small, which is also clear from the map in Fig. 4 and relates to the 16 TF coils being the source of error field. The poloidal spectrum, evaluated similarly to the RMP field, is shown in Fig. 6.

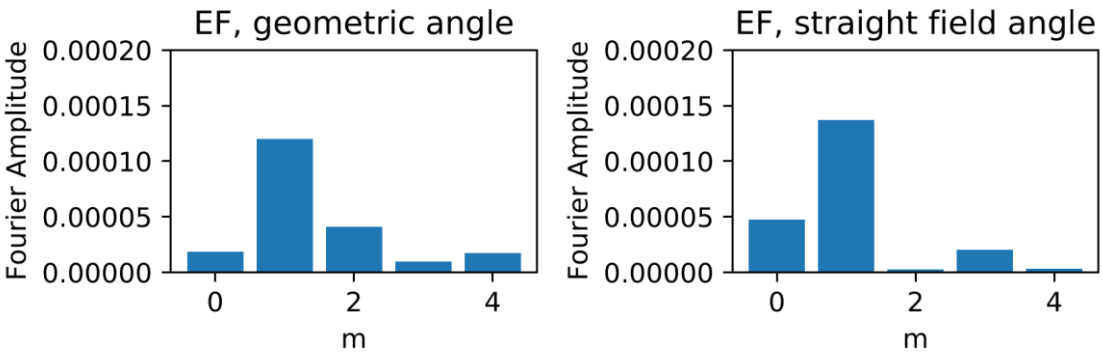

Fig. 6: Poloidal spectrum of the n=1 component of the error field shown in Fig. 4 and 5.

Similar to the RMP field, the transformation to the straight field line angle changes significantly the spectral distribution, this time moving power from the m=2 into the m=1 component. In fact, the case shown in Fig. 6 can only be poorly compensated according to the TMEI vacuum field method due to the very different distribution across the m=1,2,3 components between RMP and error field (note that the actual compensation algorithm takes into account also the phase and not only the amplitudes of the different spectral components).

Nevertheless, we can use these fields to simulate the forced rotation of tearing modes in DEMO. The 'average' error field quoted above leads to a very low $\widetilde{W}_{tot}$= 0.02 for which a mode of $\widetilde{W}_{sat}$= 0.15 locks, but the timescale for moving it around becomes large due to the quadratic dependence in Eq. (16). In Fig. 7, the temporal evolution of this case is shown. In the upper left panel, it can be seen that the mode frequency drops to zero within 5 τ_W, indicating locking from then on. The upper right panel shows the mode amplitude, which saturates around that time to the value of $\widetilde{W}_{sat}$. The lower left panel shows the phase of the applied RMP field, which starts to increase linearly on a slow time scale at 20 τ_W in an attempt to move the mode. However, the mode phase, shown in the lower right panel, does not follow the rotating RMP, indicating that the RMP force cannot overcome the braking force of the vessel in this case.

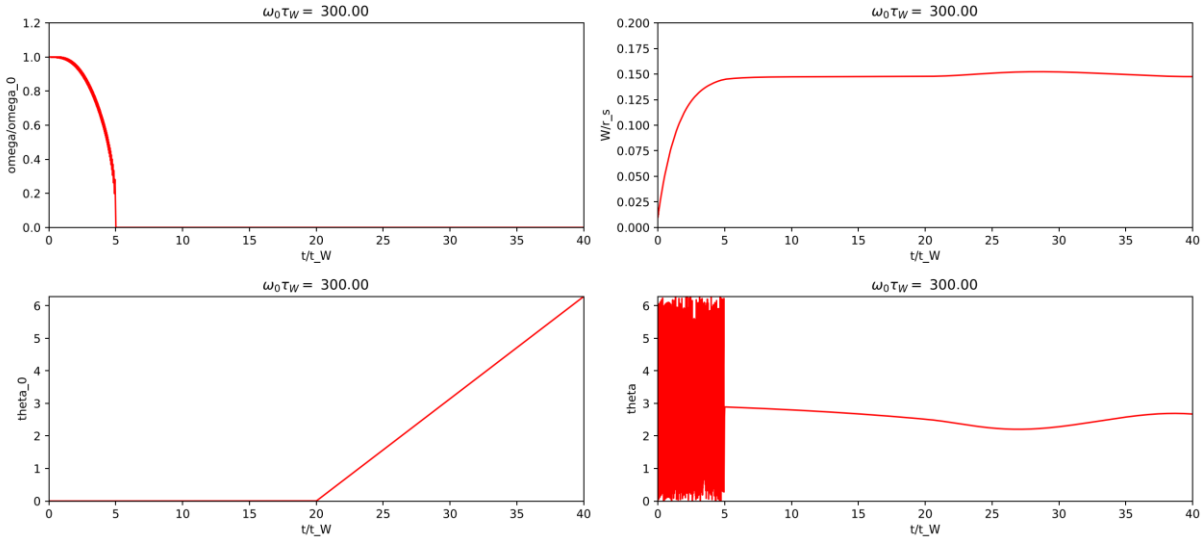

Fig. 7: Temporal evolution of mode frequency (upper left), mode amplitude (upper right), phase of the RMP field (lower left) and phase of the mode (lower right) for a case with a saturated mode amplitude of $\widetilde{W}_{sat}$= 0.15, which locks to an RMP amplitude of $\widetilde{W}_{tot}$= 0.02, but cannot be moved on a reasonable timescale if the RMP field rotates with that amplitude.

Increasing the RMP field to $\widetilde{W}_{tot}$= 0.04, the mode follows on this time scale, as can be seen in Fig. 8, in line with Eqn. (16), which predicts a threshold of 0.033 for this case. Thus, the conclusion is that at very low error field, the required amplitude of the RMP field is not given by the error field correction requirement, but rather by the time scale at which the mode should be rotated. However, this is not a problem for the presently envisaged parameters since it is well within the capability of the 3-D coils and the effect on the mode amplitude itself is very small in both cases $\widetilde{W}_{tot}$= 0.02 and $\widetilde{W}_{tot}$= 0.04, as indicated by the small change in the upper right panels after t = 20 τ_W. If we want to rotate the mode faster, e.g. on the timescale of ~ 1 second, i.e. t = 2 τ_W for the numbers used, the required $\widetilde{W}_{tot}$ increases according according to Eqn. (16). Keeping in mind that the maximum angle by which we want to move the mode is π, the required $\widetilde{W}_{tot}$will be 0.08, which increases the saturated amplitude by ~ 20 %, so it is also not advisable to exceed that value largely, but the required RMP current of around 100 kAt is now substantial, albeit still within the presently planned capabilities. We note that, in the

worst case (i.e. intrinsic error field 180 degree out of phase with the location of the ECCD launchers), this current would add to the current required for error field correction.

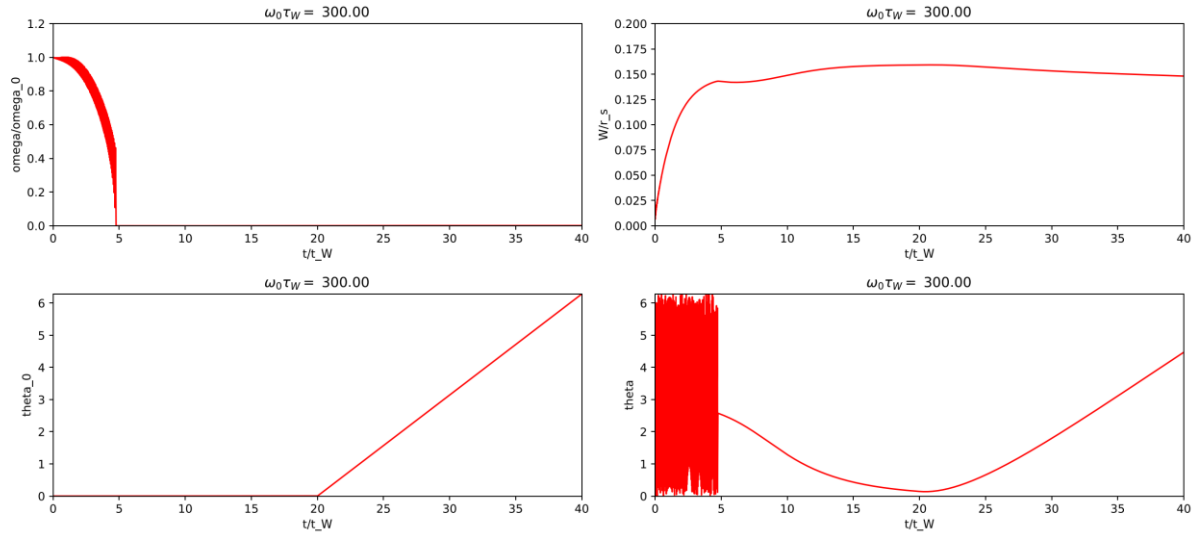

Fig. 8: Similar to Fig. 8, but now with larger RMP amplitude $\widetilde{W}_{tot}$= 0.04. At this amplitude, the mode can be moved around with by the RMP field.

4.) Summary and Conclusions

We have studied the possibility to move locked modes by applying RMP fields in DEMO. The time scale of the process is given by the damping of eddy currents in the vessel wall and decreases with increasing RMP field and mode amplitude. We find that even for the low error field expected in DEMO, the mode will lock to the error field, but in order to move the mode on a typical time scale of tearing modes, the RMP amplitude required is exceeding that needed to compensate the intrinsic error field and thus sets the requirements. In this case, moving the mode on the time scale of 1 second (the typical reaction time of the ECCD system), an RMP coil current of 100 kAt is required for a mode amplitude of $\widetilde{W}_{sat}$ = 0.15 for the EFC coils studied here and for correcting the vacuum field according to the TMEI. In the worst case (opposite phase of intrinsic error field and ECCD launchers), this would add on top of the current needed to compensate the intrinsic error field.

The results can be easily updated for other cases (e.g. other coil configurations or different error field correction strategies (e.g. ITER criterion for the plasma response SVDs) using inputs on the error field on the q=2 surface provided in the same way as in the example shown above.

5.) References

1. Zohm, H., *MHD Stability of Tokamks*. 2014, Weinheim: Wiley VCH.
2. Volpe, F.A., et al., *Avoiding Tokamak Disruptions by Applying Static Magnetic Fields That Align Locked Modes with Stabilizing Wave-Driven Currents.* Physical Review Letters, 2015. **115**(17).
3. Choi, W., et al., *Feedforward and feedback control of locked mode phase and rotation in DIII-D with application to modulated ECCD experiments.* Nuclear Fusion, 2018. **58**(3).
4. Olofsson, K.E.J., et al., *Electromechanical modelling and design for phase control of locked modes in the DIII-D tokamak.* Plasma Physics and Controlled Fusion, 2016. **58**(4).
5. Gates, D.A. and T.C. Hender, *Resistive wall induced forbidden bands of mode rotation frequency on the COMPASS-D tokamak.* Nuclear Fusion, 1996. **36**(3): p. 273-282.

6. ZOHM, H., et al., *PLASMA ANGULAR-MOMENTUM LOSS BY MHD MODE-LOCKING.* Europhysics Letters, 1990. **11**(8): p. 745-750.